JOURNAL OF CHEMICAL INFORMATION AND MODELING

Article

pubs.acs.org/jcim

Coupling of Zinc-Binding and Secondary Structure in Nonfibrillar Aβ40 Peptide Oligomerization

Liang Xu,*[,†] Shengsheng Shan,[†] Yonggang Chen,[‡] Xiaojuan Wang,[§] Ruth Nussinov,[∥,⊥] and Buyong Ma*[,⊥]

[†]School of Chemistry, [‡]Network and Information Center, and [§]School of Chemical Machinery, Dalian University of Technology, Dalian 116024, China

[∥]Sackler Institute of Molecular Medicine, Department of Human Genetics and Molecular Medicine, Sackler School of Medicine, Tel Aviv University, Tel Aviv 69978, Israel

[⊥]Basic Science Program, Leidos Biomedical Research, Inc., Cancer and Inflammation Program, National Cancer Institute, Frederick, Maryland 21702, United States

ABSTRACT: Nonfibrillar neurotoxic amyloid β (Aβ) oligomer structures are typically rich in β-sheets, which could be promoted by metal ions like Zn^{2+}. Here, using molecular dynamics (MD) simulations, we systematically examined combinations of Aβ40 peptide conformations and Zn^{2+} binding modes to probe the effects of secondary structure on Aβ dimerization energies and kinetics. We found that random conformations do not contribute to dimerization either thermodynamically or kinetically. Zn^{2+} couples with preformed secondary structures (α-helix and β-hairpin) to speed dimerization and stabilize the resulting dimer. Partial α-helices increase the dimerization speed, and dimers with α-helix rich conformations have the lowest energy. When Zn^{2+} coordinates with residues D1, H6, H13, and H14, Aβ40 β-hairpin monomers have the fastest dimerization speed. Dimers with experimentally observed zinc coordination (E11, H6, H13, and H14) form with slower rate but have lower energy. Zn^{2+} cannot stabilize fibril-like β-arch dimers. However, Zn^{2+}-bound β-arch tetramers have the lowest energy. Collectively, zinc-stabilized β-hairpin oligomers could be important in the nucleation−polymerization of cross-β structures. Our results are consistent with experimental findings that α-helix to β-structural transition should accompany Aβ aggregation in the presence of zinc ions and that Zn^{2+} stabilizes nonfibrillar Aβ oligomers and, thus, inhibits formation of less toxic Aβ fibrils.

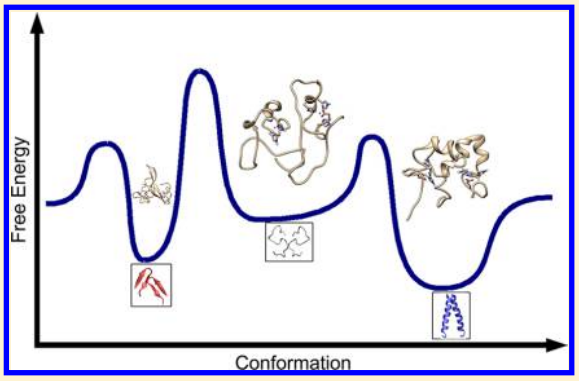

INTRODUCTION

Amyloid-β (Aβ) peptides and metal ions are two key factors in the pathology of Alzheimer's disease (AD).[1−8] Under physiological conditions, Aβ monomers primarily adopt a collapsed random coil conformation, in contrast to the cross-β-sheet structures observed in the aggregated form of mature fibrils. Aβ conformational conversion, assembly, and related biological effects have been investigated extensively.[6,9−14] It is generally believed that soluble Aβ oligomers are more neuron-toxic than mature fibrils.[7,15,16] Aβ oligomers are highly polymorphic, with the number of monomers varying from dimer to >25-mers.[15,17] Although these oligomers differ in size and morphology, all contain aggregates with appreciable β-sheet structures[11,15,17−24] or loosely aggregated strands.[25]

β-Hairpin structures along Aβ aggregation pathways are of interest because they exhibit structural motifs common in Aβ oligomers.[19,26−33] Monomeric β-hairpin structures can be detected and stabilized by binding the affibody protein[34] or by introduction of an intramolecular disulfide bond.[11,20,23,34] Itoh and Okumura[35] applied the Hamiltonian replica-permutation method to study two amyloid-β(29−42) molecules in explicit solvent. They found that random amyloid-β(29−42) molecules first form dimer and then intramolecular secondary structures, especially β-hairpins. Formation of β-hairpin structures appeared to be induced by intermolecular β-bridges. Another replica exchange simulation study,[36] demonstrated that antiparallel β-hairpins between Leu^{17}-Ala^{21}, Ala^{30}-Leu^{36}, and Val^{39}-Ile^{41}, similar to oligomer and fibril intrapeptide models, already exist in the monomer. Replica exchange simulation has also been carried out by Gnanakaran et al. They observe different dimer conformations including parallel and antiparallel orientations and relate these to secondary structural propensity of monomers.[37] However, it is unclear how the β-sheet structures evolved in the oligomers, since the β-sheet can be formed prior to oligomer formation or transformed from random or α-helical conformations, and β-hairpin conformations are generally transiently stable under physiological conditions. For example, α-helical intermediates were often observed in the aggregation process of other amyloid peptides in solution, such as amyloid β-protein (Aβ)[38] and Huntington N-terminal fragments (httNT).[39] Conversion of α-helix into β-sheet has been frequently observed in the process of amyloid formation, as in the case of the insulin[40] and designed peptides.[41]

Received: February 3, 2015
Published: May 27, 2015

DOI: 10.1021/acs.jcim.5b00063
J. Chem. Inf. Model. 2015, 55, 1218−1230

The scenario of Aβ aggregates is further complicated when considering the role of metal ions. Metal ions like Zn, Cu, and Fe can interact with Aβ peptides and have shown significant effects on Aβ aggregation.[42−45] It is still unclear how these metal ions impact Aβ oligomerization and fibrillization,[46,47] and toxicity of metal ion-induced Aβ aggregates is still in debate. For example, both sub- and superstoichiometric concentrations of Cu^{2+} have been reported to increase the formation of neurotoxic Aβ oligomers under near-physiological conditions.[48] In vitro studies have shown that Zn^{2+}−Aβ interactions stabilize nonfibrillar Aβ aggregates,[49] and these Zn^{2+}-bound Aβ oligomers are cytotoxic to cultured hippocampal neurons.[50] However, it was also reported that physiological concentrations of Cu^{2+} and Zn^{2+} ions can decrease the stability of toxic Aβ oligomers by selectively precipitating aggregation intermediates.[16,51] Recent experimental results suggest that both Cu^{2+} and Zn^{2+} ions prevent Aβ from forming fibrils but promote the formation of nonfibrillar (off-pathway) oligomers.[42] Moreover, cellular toxicity studies demonstrate that Cu^{2+} ions increase cell toxicity but Zn^{2+} ions significantly decrease the neurotoxicity of Aβ oligomers.[42] These discrepancies emphasize the importance of understanding the role of metal ions in Aβ oligomer formation.[43,52]

To date, the experimental structure of metal-bound Aβ is only available for Zn^{2+}-bound Aβ(1−16) (PDB ID: 1ZE9), with Zn^{2+} bound to His^6, Glu^{11}, His^{13}, and His^{14}.[53,54] For the two main components of full-length Aβ, Aβ40 and Aβ42, NMR data suggest that Asp^1 is the primary oxygen ligand of Zn.[22,55−57] Due to the fast kinetics of Aβ aggregation, it is experimentally challenging to characterize the Zn^{2+}-bound Aβ oligomers at the molecular level. Among the diverse Aβ oligomers, Aβ dimers are of particular importance because they can be isolated from the cortex of the AD brain,[11,58,59] and are biologically relevant building blocks of larger Aβ oligomers.[60−62]

MD simulations of Aβ dimerization have provided valuable insights into the first step of aggregation.[63−83] Several simulation studies aimed to elucidate the modulation effects that Zn ions exert on the structural and dynamics properties of Aβ monomers,[84−88] dimers,[89] and aggregates.[90,91] As an enhanced sampling method, replica-exchange molecular dynamics (REMD) simulations[92,93] have been commonly applied to efficiently sample the conformational space of Zn^{2+}-bound Aβ monomers[84−88] and aggregates under explicit or implicit solvent conditions.[90] These simulations explore mostly the properties of the conformational space of Aβ oligomers around the equilibrium. However, it is difficult to evaluate the kinetic nature of the oligomerization process. In this work, we designed combinations of three Aβ40 peptide conformations (random, partial α-helix, and β-hairpin) and two Zn^{2+} binding modes to systematically probe the effects of zinc binding and secondary structure on Aβ dimerization energies and kinetics. The selection of Aβ40 peptide instead of Aβ42 peptide is arbitrary since both Aβ40 and Aβ42 have been studied extensively, and data suggest that Zn^{2+} preferentially coordinates the N-termini. We simulate 11 Aβ(1−40) dimer systems using atomistic MD simulations in an explicit solvent environment. Our simulations indicate that while the dimer formed from two Aβ40 molecules with partial α-helical conformation has the lowest energy, a Zn^{2+}-bound β-hairpin structure is kinetically most favored to form a stable Aβ40 dimer. The β-hairpin structure becomes less stable in the absence of Zn^{2+}, suggesting that Zn^{2+} can stabilize such nonfibrillar alignment. Coupling of zinc-binding and β-hairpin structure promote the formation of nonfibrillar oligomers. While all dimers investigated in the present work are intermediate conformations along the amyloid aggregation pathway, the findings from our simulations (17 systems and total 5.76 μs) reveal important details regarding the role of secondary structures in the formation of nonfibrillar Aβ aggregates.

METHODS

The initial monomeric Zn^{2+}−Aβ40 peptides with various secondary structures including α-helix, β-hairpin, and random coil (Table 1) were selected from our previous 4-μs REMD simulations of Zn^{2+}-bound Aβ40 using the generalized Born implicit solvent model.[85] Two zinc binding modes were taken into account. In addition to three histidines (His^6, His^{13}, and His^{14}), the oxygen coordination site for Zn^{2+} is either Asp^1 or Glu^{11}. Previous experimental and MD simulation studies suggested that Zn^{2+}−Aβ40 in β-hairpin conformation is less populated.[85,87,88,94] Our previous simulations showed that the average β-sheet content of Zn^{2+}−Aβ40 is about 4.5% at 310 K.[85] Using this structure as a reference, among 100 000 (100 ns trajectory) conformations, 38 and 352 structures are found to have a C_α atom root-mean-square-deviation (RMSD) of 3.0 and 5.0 Å, respectively. Although Aβ peptides primarily adopt disordered structures in solution, for completeness, we also consider α-helix and β-hairpin conformations. In addition to one β-hairpin structure that was selected from our previous study of Zn^{2+}−Aβ40, to construct a second Zn^{2+}−Aβ40 in β-hairpin conformation the β-hairpin structure of Aβ(14−40) trapped in

Table 1. Summary of MD Simulations Performed in This Work

no.	name	system	no. of water	simulation time	initial conformations
1[a]	D1RR	$(Zn-A\beta40)_2$	26250	300 ns	coil + coil
2[a]	D1HH	$(Zn-A\beta40)_2$	24451	350 ns	helix + helix
3[a]	D1HR	$(Zn-A\beta40)_2$	24788	350 ns	helix + coil
4[a]	D1BB	$(Zn-A\beta40)_2$	22265	400 ns	β-hairpin + β-hairpin
5[b]	D2BB	$(Zn-A\beta40)_2$	46016	200 ns	β-hairpin + β-hairpin
6[b]	D2RR	$(Zn-A\beta40)_2$	19709	400 ns	coil + coil
7[b]	D2RB	$(Zn-A\beta40)_2$	27023	400 ns	β-hairpin + coil
8[b]	D2BBa	$(Zn-A\beta40)_2$	7670	800 ns	β-hairpin + β-hairpin
9	D2BBb	$(A\beta40)_2$	7666	1, 000 ns	β-hairpin + β-hairpin
10[c]	D3RB	$(Zn-A\beta40)_2$	30543	250 ns	coil + β-hairpin
11[c]	D3HR	$(Zn-A\beta40)_2$	23092	350 ns	helix + coil
12[c]	D3HB	$(Zn-A\beta40)_2$	41487	200 ns	helix + β-hairpin
13[b]	D2BBc	$(Zn-A\beta40)_2$	7657	60 ns	β-hairpin + β-hairpin[d]
14[b]	D2BBd	$(Zn-A\beta40)_2$	8048	100 ns	β-hairpin + β-hairpin[e]
15[b]	S2BB	$Zn-A\beta40$	7128	400 ns	β-hairpin + β-hairpin
16[b]	T2BBa	$(Zn-A\beta40)_4$	14303	100 ns	D2BBa + D2BBa[f]
17[b]	T2BBb	$(Zn-A\beta40)_4$	12854	100 ns	D2BBa + D2BBa[e]

[a]Zn^{2+} binds to E11, H6, H13, and H14 for these systems. [b]Zn^{2+} binds to D1, H6, H13, and H14 for these systems. [c]In addition to H6, H13, and H14, Zn^{2+} binds to E11 and D1 in the first and second monomer, respectively. [d]Fibril-like alignment. [e]Conformations were taken from ZDOCK results. [f]Two dimers in a parallel alignment similar to fibril.

DOI: 10.1021/acs.jcim.5b00063
J. Chem. Inf. Model. 2015, 55, 1218−1230

Table 2. Thermodynamic Properties (kcal/mol) of $(Zn^{2+}-A\beta40)_2$ and $(Zn^{2+}-A\beta40)_4$ Structures[a]

name	system	$G_{solvation}$	H	TS	G
D2BBa	$(Zn-A\beta40)_2$	−1272.9 (16.2)	−1629.5 (2.3)	958.8 (0.1)	−2588.3 (2.4)
D2BBd	$(Zn-A\beta40)_2$	−1100.2 (0.1)	−1478.4 (2.4)	954.2 (1.3)	−2432.6 (3.6)
T2BBb	$(Zn-A\beta40)_4$	−2423.5 (32.7)	−3302.9 (1.4)	1863.8 (1.3)	−5166.7 (2.7)
T2BBb[b]	$(Zn-A\beta40)_2$	−1489.6 (18.2)	−1608.5 (4.8)	958.5 (0.6)	−2567.0 (4.2)
T2BBb[c]	$(Zn-A\beta40)_2$	−1301.6 (24.1)	−1629.9 (4.5)	957.8 (0.0)	−2587.7 (4.5)

[a]All calculations were based on the last 50 ns trajectory of each system. The standard deviations shown in parentheses were estimated using block average method. The system names correspond to those shown in Table 1. [b]One dimer structure in the docked tetramer $(Zn-A\beta40)_4$. [c]The other dimer structure in the docked tetramer $(Zn-A\beta40)_4$.

the affibody protein (PDB ID: 2OTK)[34] was linked to Zn^{2+}-bound Aβ(1−16) (PDB ID: 1ZE9).[53] In MD studies of Zn^{2+}-bound Aβ dimer by Pan and Patterson, the two monomers are covalently linked by one Zn ion.[89] However, additional evidence suggested that Aβ aggregates induced by Zn^{2+} follow a 1:1 molar ratio of Zn^{2+} and Aβ, although the Zn^{2+}-bridged Aβ aggregates might be important metastable intermediates.[5,95] Therefore, in the present study, one zinc ion coordinates one Aβ40.

Two $Zn^{2+}-A\beta40$ monomers are separated by a distance of 60−80 Å (the distance between the center of mass of each monomer), which is about two times the length of the monomer (30−41 Å). The Aβ peptide was modeled using AMBER FF99SB force field parameters.[96] The parameters for Zn^{2+}-bound residues were taken from our previous studies.[85] Note that the partial charge on Zn^{2+} (+0.695e) is very close to the value (+0.7e) in a recent QM/MM calculation of $Zn^{2+}-A\beta16$,[47] further confirming the applicability of the present parameters. The two monomers were inserted into a box filled with TIP3P water molecules,[97] with the minimal distance between Aβ and the box border at least 45 Å. Thus, the distance between each monomer and its image due to periodic boundary conditions is ∼90 Å. Such a large water box allows $Zn^{2+}-A\beta40$ monomers to move freely at the early stage of MD simulations. Two Na^+ ions were added to neutralize the system. The system was first energy-minimized for 10 000 steps, with all atoms of $Zn^{2+}-A\beta40$ constrained to their initial positions. The system was then heated to 310 K during 25 000 steps (50 ps with an integration time step of 2 fs) and was further subjected to a 50 ps density equilibration with weak constraints on the atoms of $Zn^{2+}-A\beta40$. Langevin thermostats were applied to control the temperature at 310 K. The pressure was maintained at 1 bar using the default pressure coupling algorithm implemented in AMBER12 software. At least a 200 ns production run was performed in the NPT ensemble for each system. Snapshots from the trajectory were saved every 10 ps. For comparison, using the same protocol as stated above, both monomeric $Zn^{2+}-A\beta40$ and Zn-free $(A\beta40)_2$ in β-hairpin conformation were also simulated for 400 and 1000 ns, respectively. Based on the above monomeric and dimeric $Zn-A\beta40$ structures, we also created $(Zn^{2+}-A\beta40)_2$ and $(Zn^{2+}-A\beta40)_4$ structures based on either the NMR fibril structure (PDB ID: 2BEG)[98] or the protein−protein docking results using the ZDOCK server (http://zdock.umassmed.edu/).[99] All MD simulations were carried out using AMBER12 software,[100] and the details of the MD simulations were summarized in Table 1.

The free energy of each system was calculated in terms of the conventional MM/PBSA method.[101,102] The enthalpy contribution (H) to the free energy ($G = H - TS$) includes the internal energy (a sum of electrostatic and van der Waals interactions) and solvation free energy. The entropy (TS) was estimated using the normal-mode analysis (Table 2).The mm_pbsa.pl script in Amber12 was used to calculate the different contributions to the free energy. The desolvation free energies were calculated using Delphi, with dielectric constants for the protein and solvent set to be 1.0 and 80.0, respectively. The linear PB equation was solved by 1000 iterations with a lattice spacing in 2 grids/Å. The nonpolar solvation free energies are proportional to the solvent accessible surface area (SASA), i.e., $G_{np\text{-}solvation} = 0.0072SASA$. For the NM calculations, each conformation was energy minimized for 10 000 steps, with the convergence criterion for the energy gradient set to be 0.5 kcal/mol. The block-average method was applied to test the convergence of the MM/PBSA calculations, with the last 100 ns trajectory of each simulation divided into five parts (20 ns each). The average values and standard deviations were obtained according to the results of five MM/PBSA calculations. It was found that the minimum standard deviation is less than 5 kcal/mol for stable dimers with specific secondary structures, and ∼10 kcal/mol for dimers consisting of random coil conformation. Therefore, the largest fluctuation of free energy is ∼0.5%, indicating the convergence of our MM/PBSA calculations.

RESULTS

1. Recognition between Different Secondary Structures. *A. Recognition between Two Random Monomers.* We first investigate two systems with two starting monomers in random coil conformation, D1RR and D2RR. As can be seen in Table 1, D1RR has a zinc coordination of E11, H6, H13, and H14; and zinc coordination in D2RR is D1, H6, H13, and H14. The D1RR setup remains two separated monomers. While at certain simulation time, their distance is sufficiently close to have contact, they fluctuate to a larger separation (Figure 1A). The SASA of the hydrophobic residues remains steady around 2925.31 Å^2, and their free energies calculated in terms of MM/PBSA are higher (−2557.21 kcal/mol, Figure 2) when the simulation was terminated at 300 ns. The D2RR setup forms a dimer at around 50 ns after the simulation starts, and it remains a stable dimer in a random coil conformation (Figure 1F). The SASA gradually decreases to about 2740.81 Å^2. At the end of the simulation, the dimer has a free energy of −2503.81 kcal/mol (Figure 2).

B. Recognition between Two Helical Monomers. We select a helix-rich monomer conformation (63%) and a zinc coordination of E11, H6, H13, and H14. The D1HH setup forms a dimer after 120 ns of the simulation (Figure 1B). Similar to the D2RR dimer, the SASA of the D1HH system decreases to 2285.95 Å^2, much lower than the D2RR dimer (Figure 2).The monomer conformation used in the D1HH setup is a low energy conformation, with a free energy (for two monomers) of about −2682 kcal/mol at the beginning of the simulation, similar to that of −2693 kcal/mol for the D1RR system (Figure 1A). The energy for the D1HH dimer reached −2601.39 kcal/mol after the formation of dimer (Figure 2). As can be seen in Figure 3,

DOI: 10.1021/acs.jcim.5b00063
J. Chem. Inf. Model. 2015, 55, 1218−1230

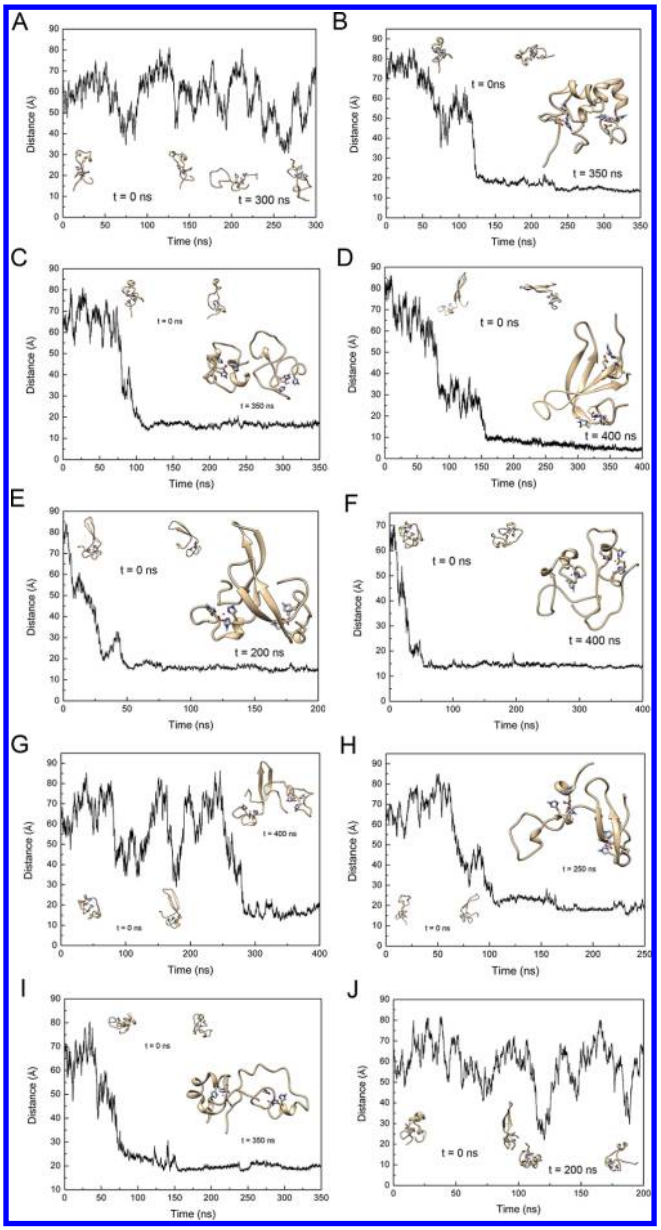

Figure 1. MD simulation of ten dimer systems: (A) D1RR, (B) D1HH, (C) D1HR, (D) D1BB, (E) D2BB, (F) D2RR, (G) D2RB, (H) D3RB, (I) D3HR, and (J) D3HB, in aqueous solution. Time evolution of the distance between the center of mass of each monomer, as well as the initial and final conformation, are shown for each system, respectively (water molecules are not shown for clarity).

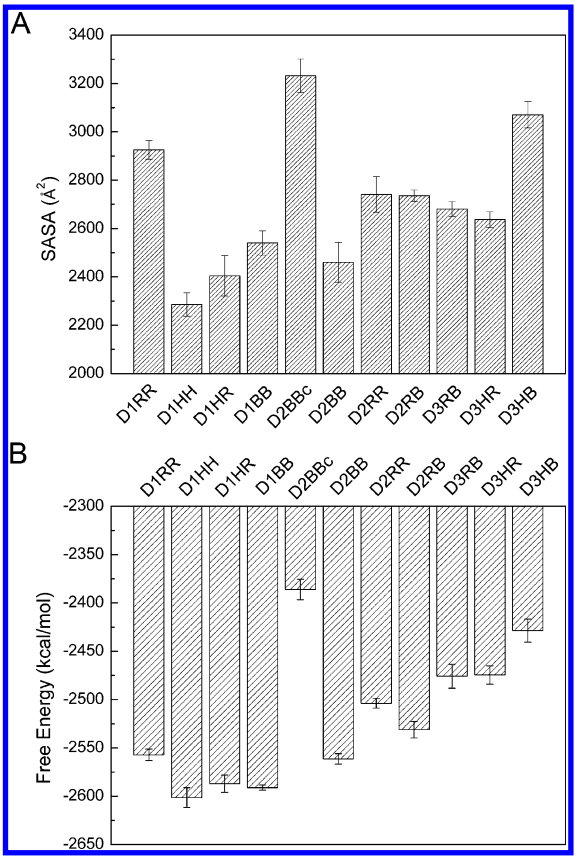

Figure 2. Solvent accessible surface area (SASA) of hydrophobic residues and free energy in terms of MM/PBSA method calculated for 11 (Zn−Aβ40)$_2$ systems. All calculations were based on the last 100 ns trajectory of each system. The standard deviations shown in parentheses were estimated using the block average method. The system names correspond to those shown in Table 1.

The RMSDs for the two monomers fluctuate around 5 Å after forming the D1HH dimer (Figure 3A). The α-helical residues still are able to maintain their conformation through 350 ns simulations (Figure 3B). The contact regions between two monomers are mainly α-helical C-terminal residues (Figure 3C and D).

C. Recognition between Two β-Hairpin Monomers. We first examine the β-hairpin monomer composed of two experimental structures (D1BB, Figure 1D). A relatively stable dimer forms after 150 ns with a SASA of 2540.36 Å^2 and a free energy of −2591.02 kcal/mol, indicating that the dimer conformation derived from two experimentally observed fragments is stable. The second β-hairpin monomer conformation was selected from a previous simulation,[85] with a different zinc coordination of D1, H6, H13, and H14 (D2BB, Figure 1E). The recognition between the two β-hairpin monomers in the D2BB setup is surprisingly fast. The two monomers quickly approach each other and begin to interact at about 41 ns and adjust to a stable conformation which lasts throughout the 200 ns simulation time. The initial hydrophobic SASA for the separated dimer is high (about 3200 Å^2), but it quickly dropped to around 2460 Å^2, comparable to that of the D1HH dimer (∼2286 Å^2). The starting free energy (∼−2439 kcal/mol) of the two β-hairpin monomers is higher than the two helical monomers. After formation of the D2BB dimer, the energy drops to −2561.40 kcal/mol and remains around this value until the end of the simulation (Figure 2).

D. Recognition between Helical and Random Monomers. We studied two systems with mixed—helical and random coil—starting conformations, D1HR (Figure 1C) and D3HR (Figure 1I). The D1HR setup has a zinc coordination of E11, H6, H13, and H14 in both monomers; in D3HR the zinc coordination includes D1, H6, H13, and H14 in the random and E11, H6, H13, and H14 in the helical monomer. As can be seen in Figure 1, dimers form similarly around 100 ns. The contact between the two monomers is more extensive and the energy much lower in the D1HR than in the D3HR dimer. The contact residues in the D1HR system do not have helical conformations, which is different from the D1HH system, where contact residues are mostly in helical conformations.

E. Recognition between the β-Hairpin and Random Monomers. Two systems with the starting conformations

DOI: 10.1021/acs.jcim.5b00063
J. Chem. Inf. Model. 2015, 55, 1218−1230

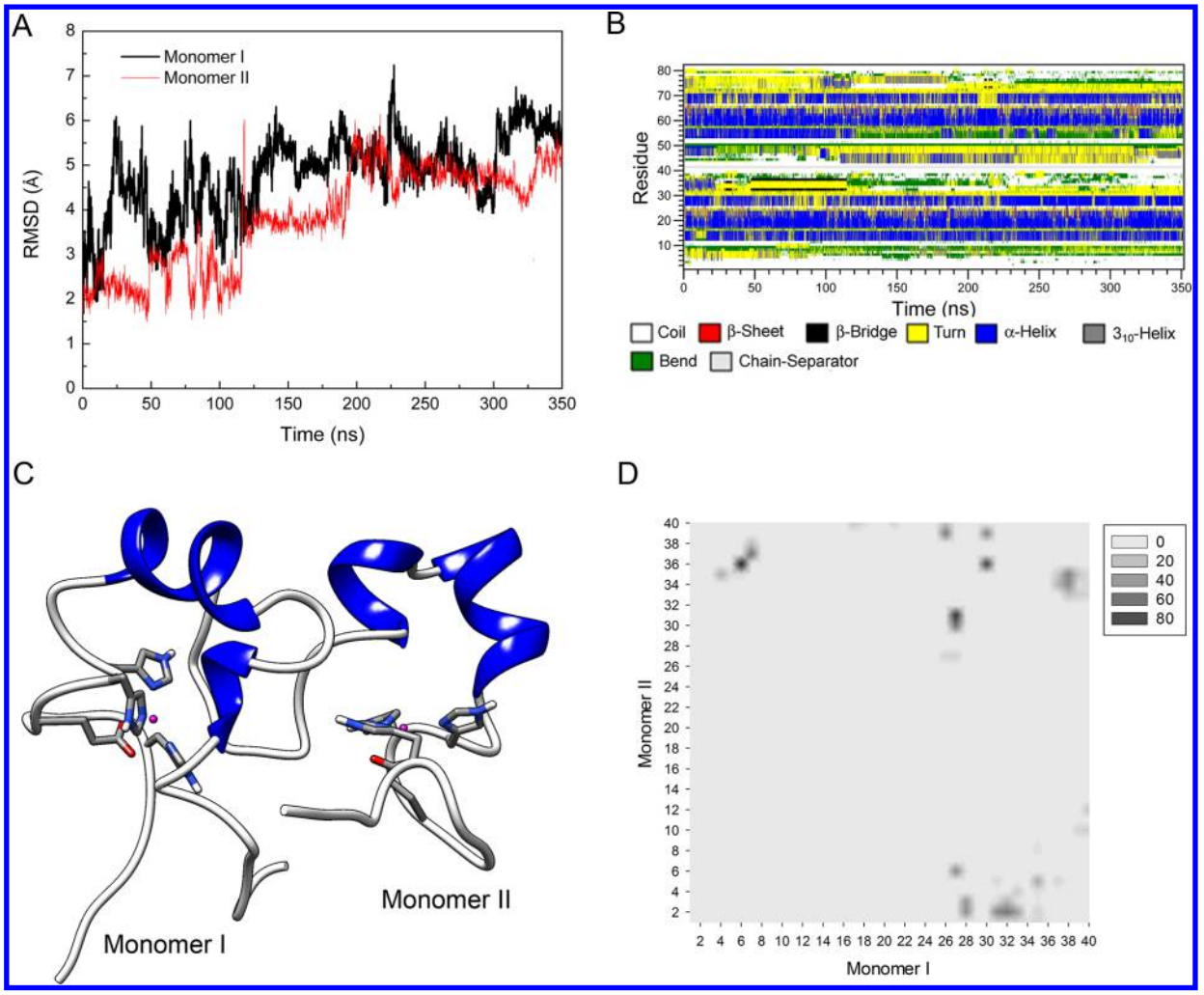

Figure 3. Results of the MD simulation of the D1HH dimer. (A) RMSD of the Cα atoms of each monomer. (B) Secondary structure change during the 350 ns MD simulation in aqueous solution. (C) Representative conformation of D1HH. (D) Contact map representing the contact frequency between two monomers. A contact occurs if the center of mass of a residue in one monomer (Monomer I) is within 6 Å of the center of mass of a residue in another monomer (Monomer II).

random coil and β-hairpin, D2RB (Figure 1G) and D3RB (Figure 1H), were simulated. All systems have the zinc coordination of D1, H6, H13, and H14 in both monomers, except that the random monomer in the D3RB has the E11, H6, H13, and H14 zinc coordination. Unlike the quick recognition between two β-hairpin monomers in the D2BB system, the dimerization of D2RB is slow, with dimer formation taking place at around 300 ns (Figure 1G). However, the D3RB dimer forms at 100 ns (Figure 1H). Both D2RB and D3RB dimers have only loose intermolecular contact, and both dimers have large SASA (about 2700 Å^2). D2RB (−2531.15 kcal/mol) has a lower free energy than the D3RB dimer (−2475.83 kcal/mol, Figure 2).

F. Recognition between the β-Hairpin and the Helical Monomers, D3HB. Finally, we examine the dimerization starting from a helical monomer (zinc binding: E11, H6, H13, and H14) and a β-hairpin monomer (zinc binding: D1, H6, H13, and H14). As can be seen in Figure 1J, our simulation did not observe the dimerization process for the D3HB system. Interestingly, during the simulation both helix and β-hairpin monomer change to random conformations (Figure 1J). As a result, the two separated monomers have the highest energy (−2428.64 kcal/mol, Figure 2) as observed in all ten combinations.

2. Zinc Traps the Metastable β-Hairpin Dimer in the Metastable High Energy Conformation. Although the dimer D1HH is rich in helical conformations and has the lowest free energy, it is interesting to see that one β-hairpin of the D1BB dimer has comparable energetics and another β-hairpin (D2BB) dimer has the fastest kinetics of formation. In this study, we are mostly interested in the β-hairpin dimers due to their potential association with toxic Aβ40 oligomers. Aβ oligomers have been suggested to be rich in β-hairpin motifs.[19] The β-hairpin structures in Aβ monomers are transiently stable,[26,34,103] raising the question of the relative stability of Zn^{2+}-bound β-hairpin structures in the monomer or oligomer states. It is thus interesting to investigate if such β-hairpin Zn^{2+}−Aβ40 dimers can self-assemble into stable oligomers.

Our simulations indicated that the β-hairpin structures are well conserved in the D1BB dimer, where each monomer interacts with other primarily through hydrophobic regions that form β-strands (Figure 4). Even though one monomer lost some β-strand during the dimerization process, the overall β-strand percentage in the dimer is maintained at around 33% at the end of simulation. As can be seen in Figure 4C, both N- and C-terminal regions contribute to the dimerization contact.

DOI: 10.1021/acs.jcim.5b00063
J. Chem. Inf. Model. 2015, 55, 1218−1230

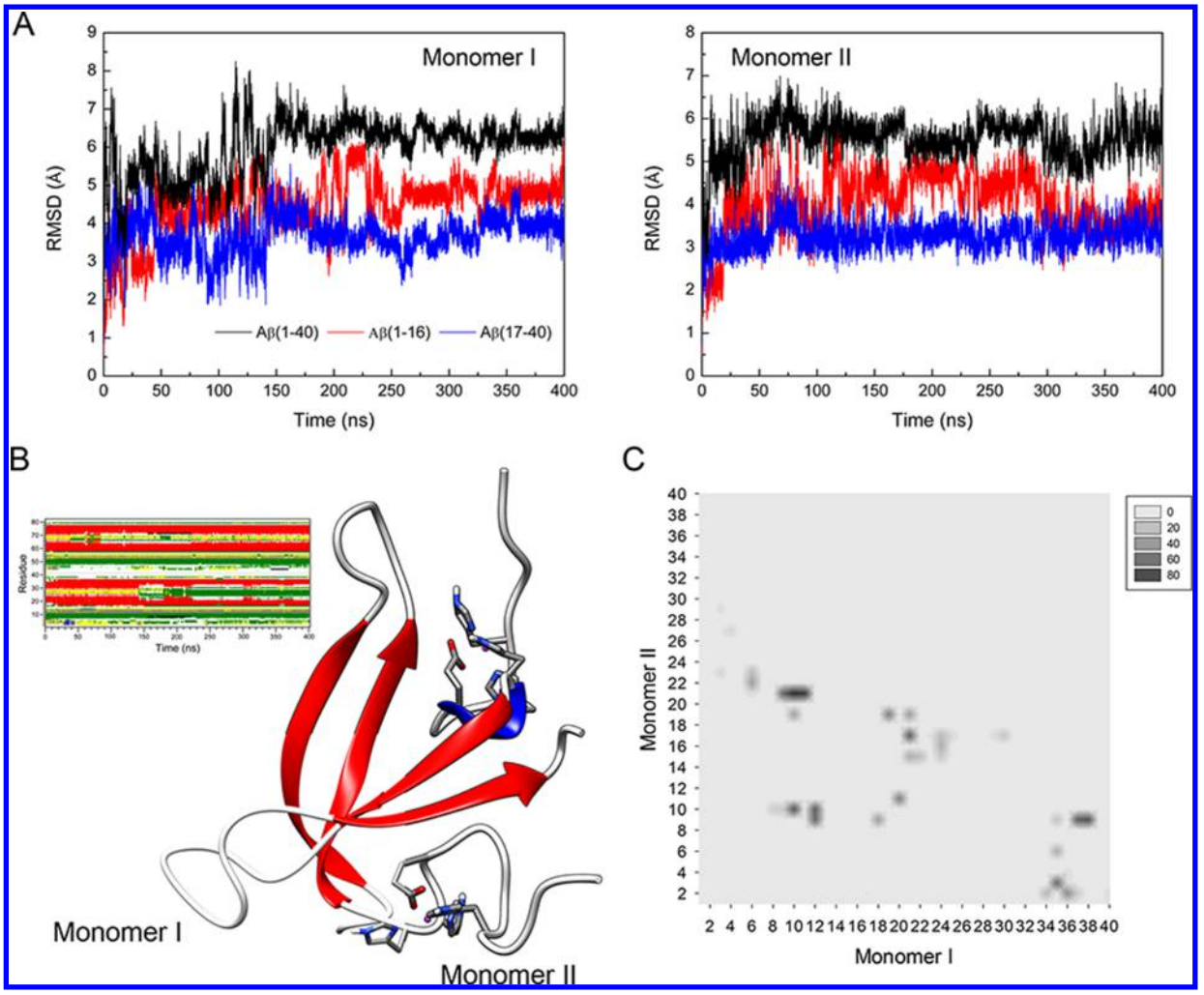

Figure 4. Analysis of the MD simulation of the D1BB dimer. (A) RMSD for different fragments of each monomer. (B) Representative conformation of D1BB, and the secondary structure change during the 400 ns MD simulation in aqueous solution. (C) Contact map representing the contact frequency between two monomers.

Beside the experimentally observed β-hairpin structure, the fast forming dimer in the D2BB setup also deserves careful examination. We extended the explicit solvent simulation of the stable β-hairpin dimer D2BB by additional 800 ns. Compared with the initial Zn^{2+}−Aβ40 conformation, the lower RMSD values of Aβ(1−16) indicate that the N-termini where Zn^{2+} binds are rather stable (Figure 5). A large RMSD fluctuation appears in one Aβ(17−40) fragment (Monomer I) during the time interval of 450−650 ns without significant alteration of the secondary structures. A closer examination shows that this β-hairpin conformation bent over during this period but bent back after 650 ns and did not display appreciable conformational changes during the remaining simulation.

Figure 6 shows that most of the backbone hydrogen bonds (HBs) are conserved when two Zn^{2+}−Aβ40 monomers self-assemble into a dimer (Figure 6A). However, there are certain variations in the interactions between the N- and C-terminals of each monomer. Specifically, in one monomer (Monomer I), the Asp^{7}-Leu^{34} pair interaction is enhanced. In another monomer (Monomer II), the occurrence of His^{13}-Leu^{34} pair interaction further increases the intramolecular interactions. The formation of intermolecular HB (Gln^{15}-Ile^{32}) is almost simultaneous with the formation of the Zn^{2+}−Aβ40 dimer. Apparently, this intermolecular HB alone is not able to stabilize the dimer. The tertiary structure of this dimer was further characterized by the contact map (Figure 6B), which indicated that intermolecular hydrophobic interactions contribute to the stability of such a dimer. These interactions expel water molecules from the region between the two hydrophobic residues-rich monomers. In contrast, the two hydrophilic N-terminals are far away and fully solvated by water molecules, preventing unfavorable electrostatic interactions. It was even found that one water molecule is stably coordinated to each Zn^{2+}ion (data not shown).

The high stability of the D2BB dimer is not observed in the standalone monomer. As described in the last section of the D3HB simulation, the isolated β-hairpin monomer is unstable (Figure 1J). We conducted an additional simulation of only the β-hairpin monomer (Figure 6C). We observed that this hairpin structure collapses in aqueous solution within 300 ns, suggesting that it is metastable in its monomeric state. The strong backbone hydrogen bonds (HBs) established between Ala^{2} and His^{6} and between Glu^{11} and His^{14} can be attributed to the binding of Zn^{2+} in the N-terminal of Aβ40. Due to the curvature in the region of Asp^{23}−Asn^{27}, permitted by the Aβ40 flexibility, the bend and turn structures interweave with each other throughout the whole 400 ns simulation.

We then test if zinc binding is necessary to stabilize the β-hairpin dimer D2BB. We start with the stable conformation, but

DOI: 10.1021/acs.jcim.5b00063
J. Chem. Inf. Model. 2015, 55, 1218−1230

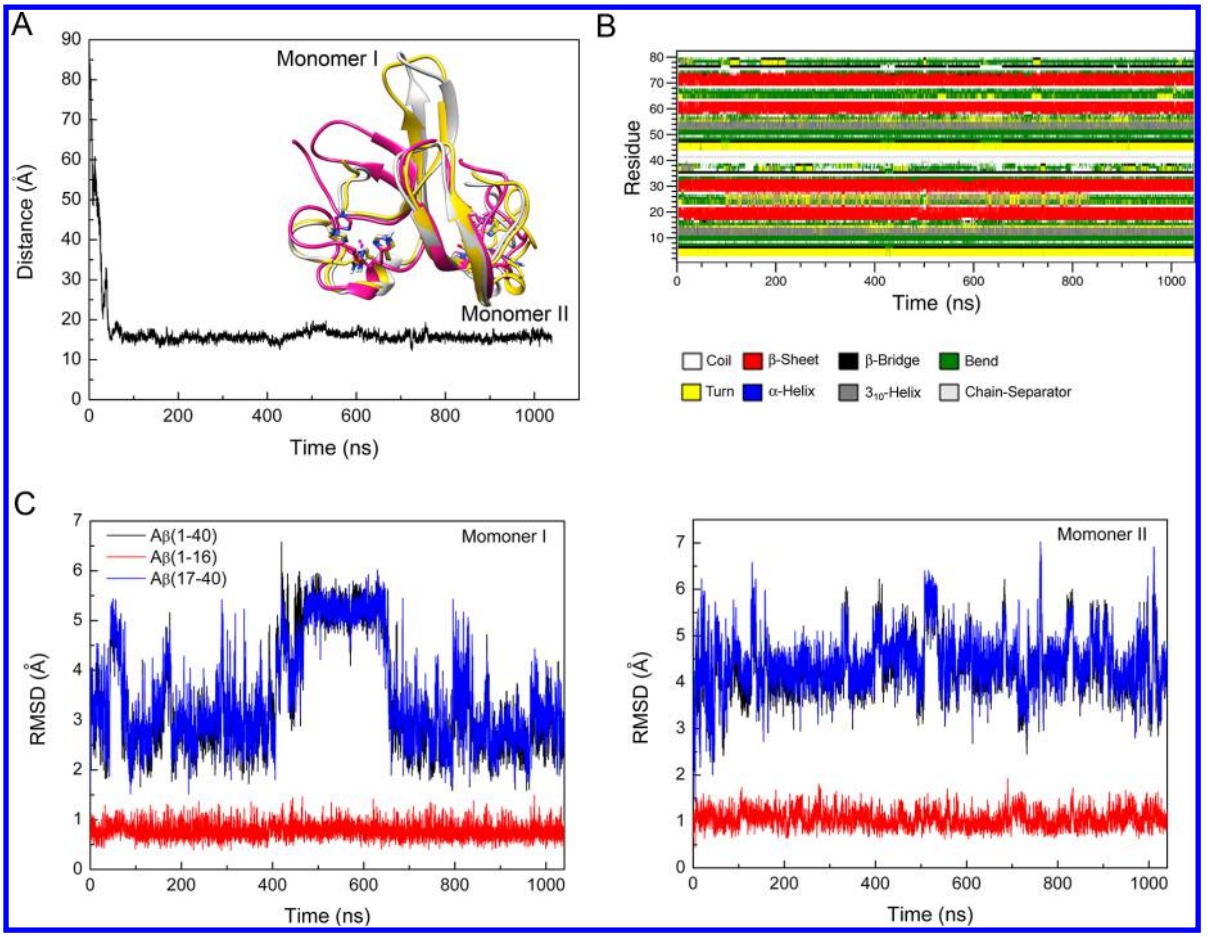

Figure 5. MD simulation of $(Zn^{2+}-A\beta40)_2$ in aqueous solution. The initial dimer was taken from the last snapshot of system D2BB. (A) Time evolution of the distance between the center of mass of each monomer over the total 1-μs MD simulation. The total simulation is 1043 ns, but the results were based on the first 1000 ns MD simulation for simplicity. (inset) Superimposition of $(Zn^{2+}-A\beta40)_2$ conformations at different time steps: t = 200 (silver), 500 (pink), and 1000 ns (yellow). (B) Secondary structure change for each residue of $(Zn^{2+}-A\beta40)_2$ structure. The gray vertical line indicates the time (t = 200 ns) at which the dimer structure was transferred from the initial large water box (D2BB in Table 1) into a smaller one (D2BBa in Table 1). (C) RMSD calculated for C_α atoms of each monomer [Aβ(1−40)]. For each monomer, RMSD values for the N-terminal [Aβ(1−16)], and the C-terminal [Aβ(17−40)] are also shown.

with zinc ions removed. In the absence of Zn^{2+}, both Aβ40 monomers show large RMSD fluctuations (Figure 7A). Although the β-hairpin conformations are largely conserved over the 1-μs MD simulation (Figure 7B), discernible alterations of the secondary structures for both monomers can be observed. In particular, transient α-helical structures can be found in the N-terminals of this Aβ40 dimer. The notable change is the realignment of two monomers within the dimer structure (Figure 7C). In contrast to the structure of $(Zn^{2+}-A\beta40)_2$, the relative orientation of the two monomers appears to be unstable and longer MD simulations are required to reach equilibrium.

3. Kinetically Stable Zinc-Containing β-Hairpin Oligomers Could Convert to Thermodynamically Stable Protofibril. The D2BB dimer optimized through a self-recognition process in our 1000 ns simulation. It is a stable Zn^{2+}-bound dimer with the fastest rate of formation. To compare with other possible β-hairpin dimers, we used the ZDOCK server to construct different dimers.[99] As indicated in Figure 8, the docked β-hairpin dimer was also subjected to 100 ns simulation (Figure 8A) and was observed to also be geometrically stable. However, the conformational energy of the docked β-hairpin dimer D2BBd is higher than the MD-optimized dimer D2BBa (Table 2), indicating that the fastest forming D2BBa dimer observed in the simulation has both kinetic and thermodynamic advantages at the given zinc binding mode.

Is the fast-forming dimer D2BBa able to form larger stable oligomers? We constructed possible Zn^{2+}-bound tetramers by dimerizing the D2BBa dimer. Two systems are simulated: the first obtained by simply aligning the D2BBa dimer (with the minimal initial distance between any atom of each unit at least 7 Å) and the second by docking two D2BBa dimers. Both tetramers are able to preserve the β-hairpin structure. However, the parallel orientation of the two dimers in the first tetramer is not stable over the 100 ns simulation (Figure 8B), compared to the docked tetramer (Figure 8C). The MM/PBSA energy of the docked tetramer is −5166.7 kcal/mol, and of two constituent dimers −2567 and −2587 kcal/mol, respectively (Table 2). The above energies indicate that the tetramerization free energy change from the dimerization of the dimer is about −12 kcal/mol. If we use the energy of the MD-optimized dimer (−2588.3 kcal/mol, Table 2) as reference, the tetramerization free energy change from the dimerization of the dimer is unfavorable by about 9 kcal/mol. Thus, tetramer formation is also only a kinetically stable process; other rearrangement may be needed to further stabilize β-hairpin tetramer.

DOI: 10.1021/acs.jcim.5b00063
J. Chem. Inf. Model. 2015, 55, 1218−1230

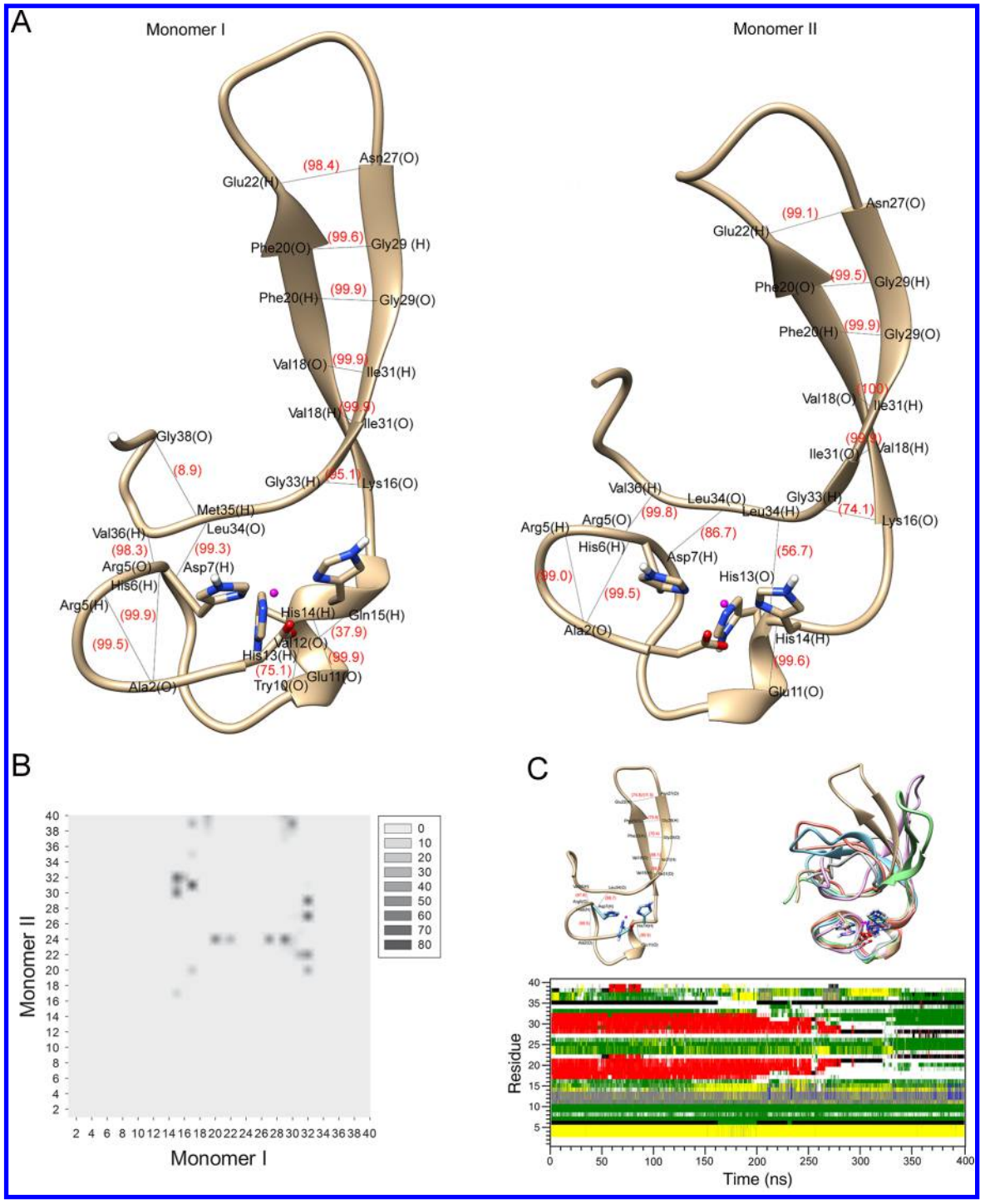

Figure 6. (A) Intramolecular HBs for each monomer of $(Zn^{2+}{-}A\beta40)_2$ in the D2BBa system (Table 1 of main text). The percentages of HBs over the total simulation are shown in parentheses. (B) Contact map showing the intermolecular interactions in $(Zn^{2+}{-}A\beta40)_2$ structure. The gray bars indicate the percentage of contacts over the MD simulation. (C) MD simulation of monomeric $Zn^{2+}{-}A\beta40$ in aqueous solution (system S2BB in Table 1 of main text). The percentages of HBs during the whole 400 ns MD simulations are shown in parentheses. For the Glu^{22}-Asn^{27} pair, the percentage of side-chain HB (11.5%) is also shown, in addition to the backbone HB percentage (74.8%). Superimposition of $Zn{-}A\beta40$ conformations at t = 0 (brown), 100 (cyan), 200 (pink), 250 (green), 300 (red), and 400 ns (gray) of the simulation. The secondary structure change for each residue is also shown. The geometric criteria implemented in Chimera[104] software was used to identify possible HBs. The distance between donor and acceptor atoms is <3 Å.

Previously, Miller et al. have shown that Zn^{2+}-bound Aβ42 octamers have stable polymorphic fibrillar states.[90] How these zinc-stabilized β-hairpin oligomers compared to the zinc-stabilized β-arch conformation in fibril? We first test if zinc binding is able to stabilize the Aβ40 dimer in fibrillar alignment. Using the D2 zinc binding mode, we linked the $Zn^{2+}{-}A\beta(1{-}16)$ N-terminal with the Aβ fibril structures (PDB ID: 2BEG) to construct a $Zn^{2+}{-}A\beta40$ dimer structure where two $Zn^{2+}{-}A\beta40$ monomers share the same alignment as the fibrillar monomers. The cross-β-sheet structures collapse on a 10 ns time-scale of the MD simulation in aqueous solution (Figure 9). Both $Zn^{2+}{-}A\beta40$ monomers become disordered and no specific pattern is found

DOI: 10.1021/acs.jcim.5b00063
J. Chem. Inf. Model. 2015, 55, 1218−1230

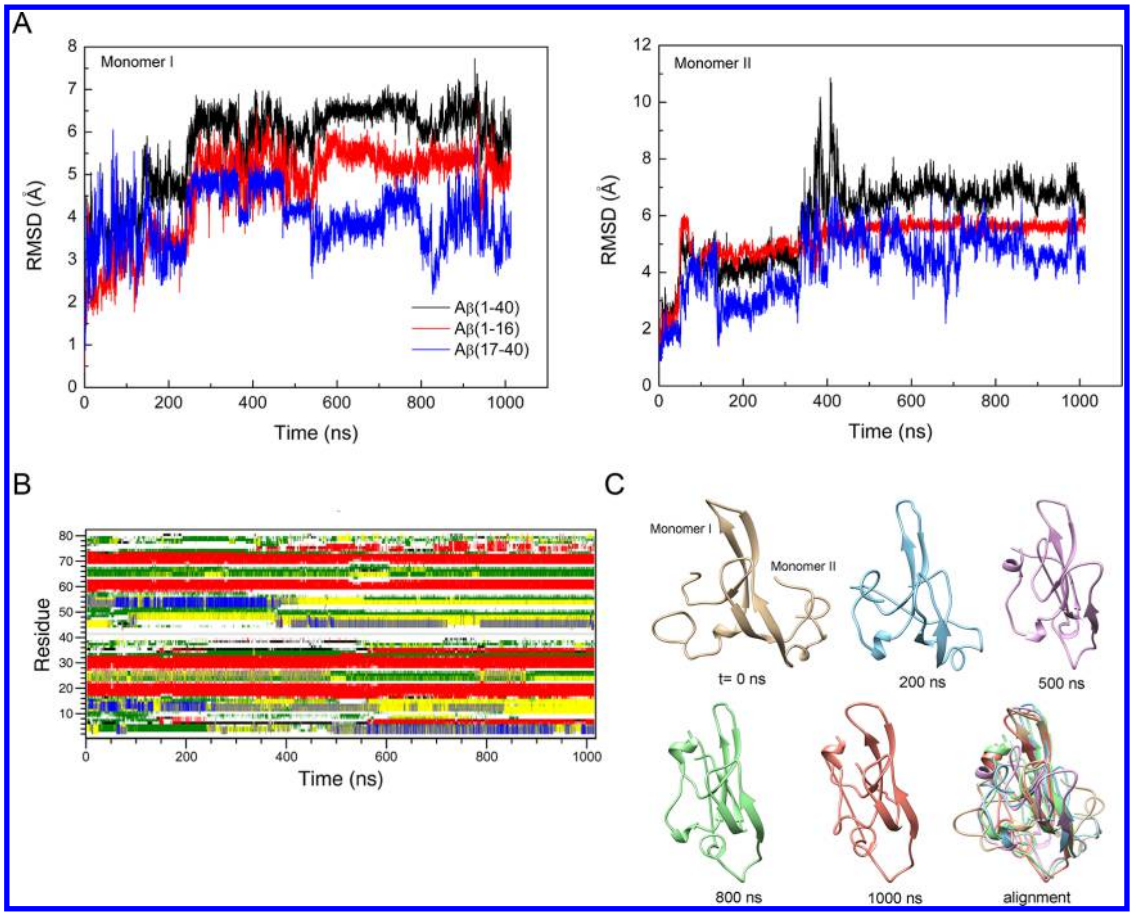

Figure 7. MD simulation of $(A\beta40)_2$ in aqueous solution (system D2BBb) in the absence of Zn^{2+}. (A) RMSD calculated for C_α atoms of each monomer [$A\beta(1-40)$]. For each monomer, RMSD values for the N-terminal [$A\beta(1-16)$] and the C-terminal [$A\beta(17-40)$] are also shown. (B) Secondary structure change for each residue of $(A\beta40)_2$ structure. The definition of secondary structures is the same as in Figure 3. (C) Representative conformations of $(A\beta40)_2$ at different times. The superimposition of these conformations is also shown. Note that the total simulation time is 1013 ns.

for their relative orientation. The energy of this collapsed dimer (−2386.08 kcal/mol, D2BBc in Figure 2) is the highest among all dimers simulated, indicating that the formation of fibrillar dimer rich in β-arch conformations is rather unfavorable. We also tested the zinc-bound $A\beta(1-16)$ N-terminal in D1 mode linked with the $A\beta$ fibril structures (PDB ID: 2BEG) at the tetramer level. Simple energy calculations indicated this zinc stabilized fibrillar tetramer has free energy around −6706 kcal/mol, indicating that fibril structure is the thermodynamically most stable state.

DISCUSSION AND CONCLUSIONS

One of the surprising observations from our simulations is that $A\beta40$ monomers separated by 60−80 Å consistently form a dimer, indicating the high tendency of $A\beta40$ oligomerization. Further, random conformations do not contribute to dimerization either thermodynamically or kinetically. In contrast, preformed secondary structures (α-helical and β-hairpin) speed the dimerization and stabilize the resulting dimer. Zinc may be coordinated by partners adopting different distorted tetrahedral geometries, stabilizing a marginally stable scaffold protein.[105] Here we show that Zn^{2+} can further stabilize the $A\beta40$ homodimer in α-helical or β-hairpin conformations. β-hairpin conformations may form dissimilar dimers with different kinetics. In the D2 binding mode (D1, H6, H13, and H14), Zn^{2+}-bound monomers dimerize quickly; in the D1 mode (E11, H6, H13, and H14), three dimers (D1HH, D1HR, and D1BB) form with slower rates but obtain lower energy. On the other hand, heterodimers with different Zn^{2+} binding modes are kinetically and energetically unfavorable.

The preformed secondary structures expose hydrophobic patches. Hydrophobic interactions between $A\beta40$ peptides appear the dominant driving force as the hydrophobic SASA decreases during the assembly process. Qi et al. studied the role of α-helix in the α-to-β transition in a fragment of the human islet amyloid polypeptide (hIAPP(11−25)), and they found that α-helix increases the intermolecular contact.[106] Barz et al. indicated that $A\beta$ can self-assemble into aggregates before conformational transition.[107] α-Helical structures were shown to be the primary component of early aggregates of the human islet amyloid polypeptide in membranes.[108] Our finding of the lowest energy dimer with α-helical contact agrees with these studies that the role of the α-helix is to increase the intermolecular contact. Further, experiment confirmed that α-to-β transition still takes place in the presence of zinc ions,[109] consistent with our current results.

Experimental[19] and computational[90,110,111] studies have shown that $A\beta$ oligomers may contain cross-β structures similar to those observed in $A\beta$ fibrils. Our studies have shown that at the dimer level, the cross-β structure cannot be stabilized. However, the cross-β structure is able to gain additional stability at the tetramer level. Clearly, the zinc stabilized β-hairpin oligomers could be important in the nucleation, polymerization, and formation of the cross-β structure. Our simulations indicate that dimerization of β-hairpin conformations contributes to the

DOI: 10.1021/acs.jcim.5b00063
J. Chem. Inf. Model. 2015, 55, 1218−1230

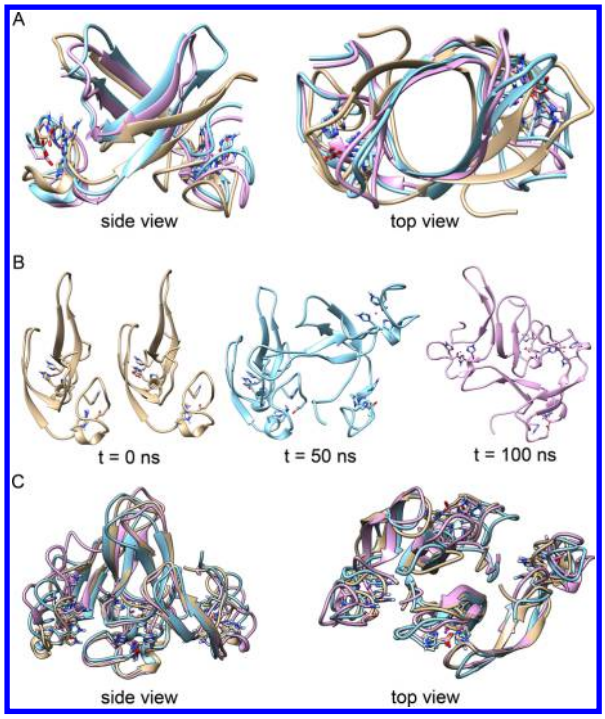

Figure 8. MD simulation of different $(Zn^{2+}–A\beta40)_2$ and $(Zn^{2+}–A\beta40)_4$ in aqueous solution. (A) Representative conformations of each system at different time steps [(t = 0 (yellow), 50 (cyan), 100 ns (purple)] are either superimposed or displayed separately. The starting conformation of $(Zn^{2+}–A\beta40)_2$ (system D2BBd) was obtained by docking two identical $Zn^{2+}–A\beta40$ structures using ZDOCK server. (B) Two $(Zn^{2+}–A\beta40)_2$ dimers are in a parallel alignment (system T2BBa), resembling the growth of Aβ aggregates along the fibril axis. (C) For system T2BBb, the starting tetramer was obtained by docking two $(Zn^{2+}–A\beta40)_2$.

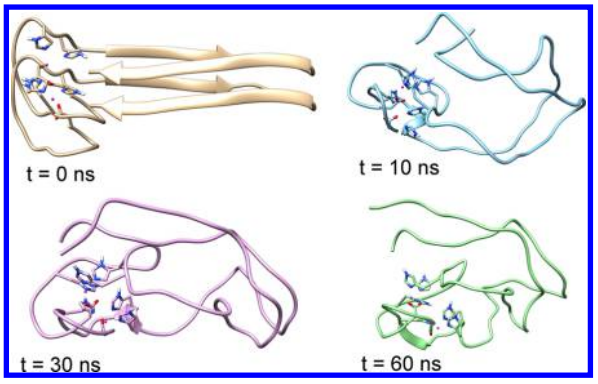

Figure 9. MD simulation of $(Zn^{2+}–A\beta40)_2$ in aqueous solution (system D2BBc). Two $Zn^{2+}–A\beta40$ monomers have the same cross β-sheet conformations and fibril-like alignment. The representative conformations of $(Zn^{2+}–A\beta40)_2$ at different time steps are shown.

stability of Aβ40. In particular, we found that self-assembly of two Zn^{2+}-bound β-hairpin conformations is coupled to the zinc binding states. We provide two examples. In the first, the C-terminal of the dimer has a β-hairpin conformation similar to that observed in a crystal structure[34] and the N-terminal coordinates zinc in a manner analogous to that observed by NMR.[53] Importantly, N-terminal region not only provides zinc coordination sites but also contribute to the interactions between two monomers. The second example relates to the fastest forming dimer, which is stable over 1-μs timescale simulation. The turn conformation of the β-hairpin in this dimer is in line with experimental observation that Zn^{2+} induces a turnlike structure in the region Val^{24}-Lys^{28} of Aβ40.[57] Recent studies suggested that this turn region is of particular importance in modulating the modes of Aβ (without Zn^{2+}) aggregation.[21,36,112−115] The absence of Glu^{22}/Asp^{23}-Lys^{28} salt-bridge in this $Zn^{2+}–A\beta40$ β-hairpin structure is also in agreement with NMR data that the binding of Zn^{2+}disrupts the Asp^{23}-Lys^{28} salt-bridge but conserves the hairpin-shaped β-structure in Aβ42 aggregates.[116]

Importantly, our tested β structures are not stable without zinc. The role of zinc can be viewed as selectively stabilizing these β-hairpin conformations. Our MD simulations show that Zn^{2+}-bound β-hairpin structures are prone to self-assemble into toxic nonfibrillar oligomers and provide a detailed scenario for the molecular mechanism of the role of Zn^{2+} and secondary structures in Aβ aggregation. As such, they validate the conjecture that metal ions like Zn^{2+} stabilize nonfibrillar Aβ oligomers and, by so doing, inhibit formation of the less toxic Aβ fibrils and favor formation of the more toxic oligomers. Zn^{2+}-bound Aβ structures promote formation of small oligomers through dimers, and these can involve different secondary structure types. Among these, Zn^{2+}-bound β-hairpin conformations play a critical role in the toxic aggregation.

Trapping Aβ peptides in β-hairpin conformations appears a sound strategy for inhibiting amyloid formation.[34,117,118] Since Aβ oligomers are more toxic than matured amyloid fibrils, inhibition of oligomer formation in Alzheimer's disease is therapeutically important. Significantly, our results indicate that it is possible to trap Aβ peptides in β-hairpin conformations. Trapping Aβ peptides and their oligomers in α-helical conformation is energetically more favorable and may be of higher therapeutic value.

AUTHOR INFORMATION

Corresponding Authors

*E-mail: xuliang@dlut.edu.cn (L.X.).
*E-mail: E-mail: mabuyong@mail.nih.gov (B.M.).

Notes

The authors declare no competing financial interest.

ACKNOWLEDGMENTS

Financial support from the Fundamental Research Funds for the Central Universities (grant no. DUT12LK38 and 2100-852018) is acknowledged. Computation time was provided by the High Performance Computing Department of Network and Information Center, Dalian University of Technology, and the high-performance computational facilities of the Biowulf PC/Linux cluster at the NIH. This project has been funded in whole or in part with Federal funds from the National Cancer Institute, National Institutes of Health, under contract number HHSN261200800001E. The content of this publication does not necessarily reflect the views or policies of the Department of Health and Human Services, nor does mention of trade names, commercial products, or organizations imply endorsement by the U.S. Government. This research was supported (in part) by the Intramural Research Program of the NIH, National Cancer Institute, Center for Cancer Research. L.X. also thanks the China Scholarship Council for financial support.

REFERENCES

(1) Hardy, J.; Selkoe, D. J. The Amyloid Hypothesis of Alzheimer's Disease: Progress and Problems on the Road to Therapeutics. *Science* **2002**, *297*, 353−356.

DOI: 10.1021/acs.jcim.5b00063
J. Chem. Inf. Model. 2015, 55, 1218−1230

(2) Goedert, M.; Spillantini, M. G. A Century of Alzheimer's Disease. *Science* **2006**, *314*, 777−781.
(3) Roberson, E. D.; Mucke, L. 100 Years and Counting: Prospects for Defeating Alzheimer's Disease. *Science* **2006**, *314*, 781−784.
(4) Rauk, A. The Chemistry of Alzheimer's Disease. *Chem. Soc. Rev.* **2009**, *38*, 2698−2715.
(5) Faller, P.; Hureau, C.; Berthoumieu, O. Role of Metal Ions in the Self-assembly of the Alzheimer's Amyloid-β Peptide. *Inorg. Chem.* **2013**, *52*, 12193−12206.
(6) Hamley, I. W. The Amyloid BetaPeptide: A Chemist's Perspective. Role in Alzheimer's and Fibrillization. *Chem. Rev.* **2012**, *112*, 5147−5192.
(7) Jang, H.; Connelly, L.; Arce, F. T.; Ramachandran, S.; Lal, R.; Kagan, B. L.; Nussinov, R. Alzheimer's Disease: Which Type of Amyloid-Preventing Drug Agents to Employ? *Phys. Chem. Chem. Phys.* **2013**, *15*, 8868−8877.
(8) Bush, A. I. The Metallobiology of Alzheimer's Disease. *Trends Neurosci.* **2003**, *26*, 207−214.
(9) Straub, J. E.; Thirumalai, D. Toward a Molecular Theory of Early and Late Events in Monomer to Amyloid Fibril Formation. *Annu. Rev. Phys. Chem.* **2011**, *62*, 437−463.
(10) Miller, Y.; Ma, B.; Nussinov, R. Polymorphism in Alzheimer AβAmyloid Organization Reflects Conformational Selection in a Rugged Energy Landscape. *Chem. Rev.* **2010**, *110*, 4820−4838.
(11) Härd, T. Protein Engineering to Stabilize Soluble Amyloid β-Protein Aggregates for Structural and Functional Studies. *FEBS J.* **2011**, *278*, 3884−3892.
(12) Xu, Y.; Shen, J. H.; Luo, X. M.; Zhu, W. L.; Chen, K. X.; Ma, J. P.; Jiang, H. L.Conformational Transition of Amyloid β-Peptide. *Proc. Natl. Acad. Sci.U. S. A.* **2005**, *102*, 5403−5407.
(13) Urbanc, B.; Betnel, M.; Cruz, L.; Bitan, G.; Teplow, D. B. Elucidation of Amyloid β-Protein Oligomerization Mechanisms: Discrete Molecular Dynamics Study. *J. Am. Chem. Soc.* **2010**, *132*, 4266−4280.
(14) Guerrero-Muñoz, M. J.; Castillo-Carranza, D. L.; Krishnamurthy, S.; Paulucci-Holthauzen, A. A.; Sengupta, U.; Lasagna-Reeves, C. A.; Ahmad, Y.; Jackson, G. R.; Kayed, R. Amyloid-β Oligomers as a Template for Secondary Amyloidosis in Alzheimer's Disease. *Neurobiol. Dis.* **2014**, *71*, 14−23.
(15) Zhao, L. N.; Long, H. W.; Mu, Y.; Chew, L. Y. The Toxicity of Amyloidβ Oligomers. *Int. J. Mol. Sci.* **2012**, *13*, 7303−7327.
(16) Garai, K.; Sahoo, B.; Kaushalya, S. K.; Desai, R.; Maiti, S. Zinc Lowers Amyloid-β Toxicity by Selectively Precipitating Aggregation Intermediates. *Biochemistry* **2007**, *46*, 10655−10663.
(17) Sakono, M.; Zako, T. Amyloid Oligomers: Formation and Toxicity of Aβ Oligomers. *FEBS J.* **2010**, *277*, 1348−1358.
(18) Stroud, J. C.; Liu, C.; Teng, P. K.; Eisenberg, D. Toxic Fibrillar Oligomers of Amyloid-β Have Cross-βStructure. *Proc. Natl. Acad. Sci.U. S. A.* **2012**, *109*, 7717−7722.
(19) Abelein, A.; Abrahams, J. P.; Danielsson, J.; Gräslund, A.; Jarvet, J.; Luo, J.; Tiiman, A.; Wärmländer, S. K. T. S. The Hairpin Conformation of the Amyloid β Peptide Is an Important Structural Motif Along the Aggregation Pathway. *J. Biol. Inorg. Chem.* **2014**, *19*, 623−634.
(20) Yu, L.; Edalji, R.; Harlan, J. E.; Holzman, T. F.; Lopez, A. P.; Labkovsky, B.; Hillen, H.; Barghorn, S.; Ebert, U.; Richardson, P. L.; Miesbauer, L.; Solomon, L.; Bartley, D.; Walter, K.; Johnson, R. W.; Hajduk, P. J.; Olejniczak, E. T. Structural Characterization of a Soluble Amyloid β-Peptide Oligomer. *Biochemistry* **2009**, *48*, 1870−1877.
(21) Rezaei-Ghaleh, N.; Amininasab, M.; Giller, K.; Kumar, S.; Stündl, A.; Schneider, A.; Becker, S.; Walter, J.; Zweckstetter, M. Turn Plasticity Distinguishes Different Modes of Amyloid-β Aggregation. *J. Am. Chem. Soc.* **2014**, *136*, 4913−4919.
(22) Danielsson, J.; Pierattelli, R.; Banci, L.; Gräslund, A. High-Resolution NMR Studies of the Zinc-Binding Site of the Alzheimer's Amyloid β-Peptide. *FEBS J.* **2007**, *274*, 46−59.
(23) Sandberg, A.; Luheshi, L. M.; Sollvander, S.; Pereira de Barros, T.; Macao, B.; Knowles, T. P. J.; Biverstal, H.; Lendel, C.; Ekholm-Petterson, F.; Dubnovitsky, A.; Lannfelt, L.; Dobson, C. M.; Hard, T. Stabilization of Neurotoxic Alzheimer Amyloid-β Oligomers by Protein Engineering. *Proc. Natl. Acad. Sci.U. S. A.* **2010**, *107*, 15595−15600.
(24) Suzuki, Y.; Brender, J. R.; Soper, M. T.; Krishnamoorthy, J.; Zhou, Y.; Ruotolo, B. T.; Kotov, N. A.; Ramamoorthy, A.; Marsh, E. N. G. Resolution of Oligomeric Species during the Aggregation of $A\beta_{1-40}$ using ^{19}F NMR. *Biochemistry* **2013**, *52*, 1903−1912.
(25) Ahmed, M.; Davis, J.; Aucoin, D.; Sato, T.; Ahuja, S.; Aimoto, S.; Elliott, J. I.; Van Nostrand, W. E.; Smith, S. O.Structural Conversion of Neurotoxic Amyloid-β_{1-42} Oligomers to Fibrils. *Nat. Struct. Mol. Biol.* **2010**, *17*, 561−567.
(26) Cruz, L.; Rao, J. S.; Teplow, D. B.; Urbanc, B. Dynamics of Metastable β-Hairpin Structures in the Folding Nucleus of Amyloid β-Protein. *J. Phys. Chem. B* **2012**, *116*, 6311−56325.
(27) Larini, L.; Shea, J. E. Role of β-Hairpin Formation in Aggregation: The Self-Assembly of the Amyloid-β(25−35) Peptide. *Biophys. J.* **2012**, *103*, 576−5586.
(28) Mithu, V. S.; Sarkar, B.; Bhowmik, D.; Das, A. K.; Chandrakesan, M.; Maiti, S.; Madhu, P. K. Curcumin Alters the Salt Bridge-Containing Turn Region in Amyloid β (1−42) Aggregates. *J. Biol. Chem.* **2014**, *289*, 11122−11131.
(29) Ma, B. Y.; Nussinov, R. Stabilities and Conformations of Alzheimer's Beta-Amyloid Peptide Oligomers (Aβ(16−22) Aβ(16−35) and Aβ(10−35)): Sequence Effects. *Proc. Natl. Acad. Sci.U. S. A.* **2002**, *99*, 14126−14131.
(30) Ma, B. Y.; Nussinov, R. Molecular Dynamics Simulations of Alanine Rich β-Sheet Oligomers: Insight Into Amyloid Formation. *Protein Sci.* **2002**, *11*, 2335−2350.
(31) Jang, H.; Arce, F. T.; Ramachandran, S.; Kagan, B. L.; Lal, R.; Nussinov, R. Disordered Amyloidogenic Peptides May Insert into the Membrane and Assemble into Common Cyclic Structural Motifs. *Chem. Soc. Rev.* **2014**, *43*, 6750−6764.
(32) Jang, H.; Arce, F. T.; Ramachandran, S.; Kagan, B. L.; Lal, R.; Nussinov, R. Familial Alzheimer's Disease Osaka Mutant (ΔE22) β-Barrels Suggest an Explanation for the Different Aβ(1−40/42) Preferred Conformational States Observed by Experiment. *J. Phys. Chem. B* **2013**, *117*, 11518−11529.
(33) Guerrero-Muñoz, M. J.; Castillo-Carranza, D. L.; Sengupta, U.; White, M. A.; Kayed, R. Design of Metastable β-Sheet Oligomers from Natively Unstructured Peptide. *ACS Chem. Neurosci.* **2013**, *4*, 1520−1523.
(34) Hoyer, W.; Gronwall, C.; Jonsson, A.; Stahl, S.; Hard, T. Stabilization of A β-Hairpin in Monomeric Alzheimer's Amyloid-β Peptide Inhibits Amyloid Formation. *Proc. Natl. Acad. Sci.U. S. A.* **2008**, *105*, 5099−5104.
(35) Itoh, S. G.; Okumura, H. Dimerization Process of Amyloid-β(29−42) Studied by the Hamiltonian Replica-Permutation Molecular Dynamics Simulations. *J. Phys. Chem. B* **2014**, *118*, 11428−11436.
(36) Rosenman, D. J.; Connors, C. R.; Chen, W.; Wang, C.; Garcia, A. E. Aβ Monomers Transiently Sample Oligomer and Fibril-Like Configurations: Ensemble Characterization using a Combined MD/NMR Approach. *J. Mol. Biol.* **2013**, *425*, 3338−3359.
(37) Gnanakaran, S.; Nussinov, R.; Garcia, A. E. Atomic-Level Description of Amyloid-β Dimer Formation. *J. Am. Chem. Soc.* **2006**, *128*, 2158−2159.
(38) Kirkitadze, M. D.; Condron, M. M.; Teplow, D. B. Identification and Characterization of Key Kinetic Intermediates in Amyloid β-Protein Fibrillogenesis. *J. Mol. Biol.* **2001**, *312*, 1103−1119.
(39) Jayaraman, M.; Kodali, R.; Sahoo, B.; Thakur, A. K.; Mayasundari, A.; Mishra, R.; Peterson, C. B.; Wetzel, R. Slow Amyloid Nucleation Via α-Helix-Rich Oligomeric Intermediates in Short Polyglutamine-Containing Huntingtin Fragments. *J. Mol. Biol.* **2012**, *415*, 881−899.
(40) Yamamoto, S.; Watarai, H. Raman Optical Activity Study on Insulin Amyloidand Prefibril Intermediate. *Chirality* **2012**, *24*, 97−103.
(41) Singh, Y.; Sharpe, P. C.; Hoang, H. N.; Lucke, A. J.; McDowall, A. W.; Bottomley, S. P.; Fairlie, D. P. Amyloid Formation From an α-Helix Peptide Bundle is Seeded by 3_{10}-Helix Aggregates. *Chem.—Eur. J.* **2011**, *17*, 151−160.

DOI: 10.1021/acs.jcim.5b00063
J. Chem. Inf. Model. 2015, 55, 1218−1230

(42) Sharma, A. K.; Pavlova, S. T.; Kim, J.; Kim, J.; Mirica, L. M. The Effect of Cu^{2+} and Zn^{2+} on the Aβ42 Peptide Aggregation and Cellular Toxicity. *Metallomics* **2013**, *5*, 1529−1536.
(43) Faller, P.; Hureau, C.; La Penna, G. Metal Ions and Intrinsically Disordered Proteins and Peptides: From Cu/Zn Amyloid-β to General Principles. *Acc. Chem. Res.* **2014**, *47*, 2252−2259.
(44) Miller, Y.; Ma, B.; Nussinov, R. Metal Binding Sites in Amyloid Oligomers: Complexes and Mechanisms. *Coord. Chem. Rev.* **2012**, *256*, 2245−2252.
(45) Parthasarathy, S.; Long, F.; Miller, Y.; Xiao, Y. L.; McElheny, D.; Thurber, K.; Ma, B. Y.; Nussinov, R.; Ishii, Y. Molecular-Level Examination of Cu^{2+} Binding Structure for Amyloid Fibrils of 40-Residue Alzheimer's β by Solid-State NMR Spectroscopy. *J. Am. Chem. Soc.* **2011**, *133*, 3390−3400.
(46) Carloni, P.; Kahler, A.; Sticht, H.; Horn, A. H. C. Conformational Stability of Fibrillar Amyloid-β Oligomers via Protofilament Pair Formation−A Systematic Computational Study. *PLoS One* **2013**, *8*, e70521.
(47) Maiorana, A.; Marino, T.; Minicozzi, V.; Morante, S.; Russo, N. A Micro-Environmental Study of the Zn^{+2}−Aβ_{1-16} Structural Properties. *Biophys. Chem.* **2013**, *182*, 86−93.
(48) Mold, M.; Ouro-Gnao, L.; Wieckowski, B. M.; Exley, C. Copper Prevents Amyloid-β_{1-42} from Forming Amyloid Fibrils under near-Physiological Conditions in Vitro. *Sci. Rep.* **2013**, *3*, 1256.
(49) Noy, D.; Solomonov, I.; Sinkevich, O.; Arad, T.; Kjaer, K.; Sagi, I. Zinc-Amyloid β Interactions on a Millisecond Time-Scale Stabilize Mon-Fibrillar Alzheimer-Related Species. *J. Am. Chem. Soc.* **2008**, *130*, 1376−1383.
(50) Solomonov, I.; Korkotian, E.; Born, B.; Feldman, Y.; Bitler, A.; Rahimi, F.; Li, H.; Bitan, G.; Sagi, I. Zn^{2+}−Aβ40 Complexes form Metastable Quasi-Spherical Oligomers That Are Cytotoxic to Cultured Hippocampal Neurons. *J. Biol. Chem.* **2012**, *287*, 20555−20564.
(51) Garai, K.; Sengupta, P.; Sahoo, B.; Maiti, S. Selective Destabilization of Soluble Amyloid β Oligomers by Divalent Metal Ions. *Biochem. Biophys. Res. Commun.* **2006**, *345*, 210−215.
(52) Savelieff, M. G.; Liu, Y. Z.; Senthamarai, R. R. P.; Korshavn, K. J.; Lee, H. J.; Ramamoorthy, A.; Lim, M. H. A Small Molecule that Displays Marked Reactivity Toward Copper- Versus Zinc-Amyloid-βImplicated in Alzheimer's Disease. *Chem. Commun.* **2014**, *50*, 5301−5303.
(53) Zirah, S.; Kozin, S. A.; Mazur, A. K.; Blond, A.; Cheminant, M.; Segalas-Milazzo, I.; Debey, P.; Rebuffat, S. Structural Changes of Region 1−16 of the Alzheimer Disease Amyloid β-Peptide upon Zinc Binding and in Vitro Aging. *J. Biol. Chem.* **2005**, *281*, 2151−2161.
(54) Tsvetkov, P. O.; Kulikova, A. A.; Golovin, A. V.; Tkachev, Y. V.; Archakov, A. I.; Kozin, S. A.; Makarov, A. A. Minimal Zn^{2+} Binding Site of Amyloid-β. *Biophys. J.* **2010**, *99*, L84−L86.
(55) Faller, P.; Hureau, C. Bioinorganic Chemistry of Copper and Zinc Ions Coordinated to Amyloid-β Peptide. *Dalton Trans.* **2009**, 1080−1094.
(56) Tõugu, V.; Tiiman, A.; Palumaa, P. Interactions of Zn(II) and Cu(II) Ions with Alzheimer'sAmyloid-βPeptide. Metal Ion Binding, Contribution to Fibrillization and Toxicity. *Metallomics* **2011**, *3*, 250.
(57) Rezaei-Ghaleh, N.; Giller, K.; Becker, S.; Zweckstetter, M. Effect of Zinc Binding on β-Amyloid Structure and Dynamics: Implications for Aβ Aggregation. *Biophys. J.* **2011**, *101*, 1202−1211.
(58) Shankar, G. M.; Li, S.; Mehta, T. H.; Garcia-Munoz, A.; Shepardson, N. E.; Smith, I.; Brett, F. M.; Farrell, M. A.; Rowan, M. J.; Lemere, C. A.; Regan, C. M.; Walsh, D. M.; Sabatini, B. L.; Selkoe, D. J. Amyloid-β Protein Dimers Isolated Directly from Alzheimer's Brains Impair Synaptic Plasticity and Memory. *Nat. Med.* **2008**, *14*, 837−842.
(59) Jin, M.; Shepardson, N.; Yang, T.; Chen, G.; Walsh, D.; Selkoe, D. J. Soluble Amyloid β-Protein Dimers Isolated from Alzheimer Cortex directly Induce Tau Hyperphosphorylation and Neuritic Degeneration. *Proc. Natl. Acad. Sci.U. S. A.* **2011**, *108*, 5819−5824.
(60) Lopez del Amo, J. M.; Schmidt, M.; Fink, U.; Dasari, M.; Fändrich, M.; Reif, B. An Asymmetric Dimer as the Basic Subunit in Alzheimer's Disease Amyloid β Fibrils. *Angew. Chem., Int. Ed.* **2012**, *51*, 6136−6139.
(61) O'Nuallain, B.; Freir, D. B.; Nicoll, A. J.; Risse, E.; Ferguson, N.; Herron, C. E.; Collinge, J.; Walsh, D. M. Amyloid β-Protein Dimers Rapidly Form Stable Synaptotoxic Protofibrils. *J. Neurosci.* **2010**, *30*, 14411−14419.
(62) Lv, Z.; Roychaudhuri, R.; Condron, M. M.; Teplow, D. B.; Lyubchenko, Y. L. Mechanism of Amyloid β-Protein Dimerization Determined Using Single-Molecule AFM Force Spectroscopy. *Sci. Rep.* **2013**, *3*, 2880.
(63) Zheng, J.; Manna, M.; Mukhopadhyay, C. Dimer Formation Enhances Structural Dfferences between Amyloid β-Protein (1−40) and (1−42): An Explicit-Solvent Molecular Dynamics Study. *PLoS One* **2012**, *7*, e34345.
(64) Zhu, X.; Bora, R. P.; Barman, A.; Singh, R.; Prabhakar, R. Dimerization of the Full-Length Alzheimer Amyloid β-Peptide (Aβ42) in Explicit Aqueous Solution: AMolecular Dynamics Study. *J. Phys. Chem. B* **2012**, *116*, 4405−4416.
(65) Yano, A.; Okamoto, A.; Nomura, K.; Higai, S. i.; Kurita, N. Difference in Dimer Conformation between Amyloid-β(1−42) and (1−43) Proteins: Replica Exchange Molecular Dynamics Simulations in Water. *Chem. Phys. Lett.* **2014**, 595−596.
(66) Müller-Schiffmann, A.; Andreyeva, A.; Horn, A. H. C.; Gottmann, K.; Korth, C.; Sticht, H. Molecular Engineering of a Secreted, Highly Homogeneous, and Neurotoxic Aβ Dimer. *ACS Chem. Neurosci.* **2011**, *2*, 242−248.
(67) Zheng, J.; Manna, M.; Mukhopadhyay, C. Binding, Conformational Transition and Dimerization of Amyloid-β Peptide on GM1-Containing Ternary Membrane: Insights from Molecular Dynamics Simulation. *PLoS One* **2013**, *8*, e71308.
(68) Hwang, W.; Zhang, S.; Kamm, R. D.; Karplus, M. Kinetic Control of Dimer Structure Formation in Amyloid Fibrillogenesis. *Proc. Natl. Acad. Sci.U. S. A.* **2004**, *101*, 12916−12921.
(69) Anand, P.; Nandel, F. S.; Hansmann, U. H. E. The Alzheimer β-Amyloid (Aβ_{1-39}) Dimer in an Implicit Solvent. *J. Chem. Phys.* **2008**, *129*, 195102.
(70) Jang, S.; Shin, S. Amyloid β-Peptide Oligomerizationinsilico: Dimer and Trimer. *J. Phys. Chem. B* **2006**, *110*, 1955−1958.
(71) Chong, S. H.; Ham, S. Impact of Chemical Heterogeneity on Protein Self-Assembly in Water. *Proc. Natl. Acad. Sci.U. S. A.* **2012**, *109*, 7636−7641.
(72) Côté, S.; Laghaei, R.; Derreumaux, P.; Mousseau, N. Distinct Dimerization for Various Alloforms of the Amyloid-β Protein: Aβ1−40, Aβ1−42, and Aβ1−40(D23N). *J. Phys. Chem. B* **2012**, *116*, 4043−4055.
(73) Urbanc, B.; Cruz, L.; Ding, F.; Sammond, D.; Khare, S.; Buldyrev, S. V.; Stanley, H. E.; Dokholyan, N. V. Molecular Dynamics Simulation of Amyloid β Dimer Formation. *Biophys. J.* **2004**, *87*, 2310−2321.
(74) Zhang, T.; Zhang, J.; Derreumaux, P.; Mu, Y. Molecular Mechanism of the Inhibition of EGCG on the Alzheimer Aβ_{1-42}Dimer. *J. Phys. Chem. B* **2013**, *117*, 3993−4002.
(75) Viet, M. H.; Nguyen, P. H.; Ngo, S. T.; Li, M. S.; Derreumaux, P. Effect of the Tottori Familial Disease Mutation (D7N) on the Monomers and Dimers of Aβ40 and Aβ42. *ACS Chem. Neurosci.* **2013**, *4*, 1446−1457.
(76) Zhang, T.; Xu, W. X.; Mu, Y. G.; Derreumaux, P. Atomic and Dynamic Insights into the Beneficial Effect of the 1,4-Naphthoquinon-2-yl-l-tryptophan Inhibitor on Alzheimer's Aβ_{1-42}Dimer in Terms of Aggregation and Toxicity. *ACS Chem. Neurosci.* **2014**, *5*, 148−159.
(77) Viet, M. H.; Nguyen, P. H.; Derreumaux, P.; Li, M. S. Effect of the English Familial Disease Mutation (H6R) on the Monomers and Dimers of Aβ40 and Aβ42. *ACS Chem. Neurosci.* **2014**, *5*, 646−657.
(78) Huet, A.; Derreumaux, P. Impact of the Mutation A21G (Flemish Variant) on Alzheimer's β-Amyloid Dimers by Molecular Dynamics Simulations. *Biophys. J.* **2006**, *91*, 3829−3840.
(79) Lockhart, C.; Kim, S.; Kumar, R.; Klimov, D. K. Does Amino Acid Sequence Determine the Properties of Aβ Dimer? *J. Chem. Phys.* **2011**, *135*, 035103.
(80) Wei, G.; Jewett, A. I.; Shea, J.-E. Structural Diversity of Dimers of the Alzheimer Amyloid-β(25−35) Peptide and Polymorphism of the Resulting Fibrils. *Phys. Chem. Chem. Phys.* **2010**, *12*, 3622−3629.
(81) Zhao, L. N.; Chiu, S.-W.; Benoit, J.; Chew, L. Y.; Mu, Y. The Effect of Curcumin on the Stability of Aβ Dimers. *J. Phys. Chem. B* **2012**, *116*, 7428−7435.

DOI: 10.1021/acs.jcim.5b00063
J. Chem. Inf. Model. 2015, 55, 1218−1230

(82) Chong, S.-H.; Ham, S. Atomic-Level Investigations on the Amyloid-β Dimerization Process and Its Driving Forces in Water. *Phys. Chem. Chem. Phys.* **2012**, *14*, 1573−1575.
(83) Lu, S.; Li, S.; Zhang, J. Harnessing Allostery: A Novel Approach to Drug Discovery. *Med. Res. Rev.* **2014**, *34*, 1242−1285.
(84) Li, W.; Zhang, J.; Su, Y.; Wang, J.; Qin, M.; Wang, W. Effects of Zinc Binding on the Conformational Distribution of the Amyloid-β Peptide Based on Molecular Dynamics Simulations. *J. Phys. Chem. B* **2007**, *111*, 13814−13821.
(85) Xu, L.; Wang, X.; Wang, X. Effects of Zn^{2+} Binding on the Structural and Dynamic Properties of Amyloid β Peptide Associated with Alzheimer's Disease: Asp^{1}or Glu^{11}? *ACS Chem. Neurosci.* **2013**, *4*, 1458−1468.
(86) Xu, L.; Wang, X. J.; Wang, X. C. Characterization of the Internal Dynamics and Conformational Space of Zinc-Bound Amyloid β Peptides by Replica-Exchange Molecular Dynamics Simulations. *Eur. Biophys. J.* **2013**, *42*, 575−586.
(87) Wise-Scira, O.; Xu, L.; Perry, G.; Coskuner, O. Structures and Free Energy Landscapes of Aqueous Zinc(II)-Bound Amyloid-β(1−40) and Zinc(II)-Bound Amyloid-β(1−42) with Dynamics. *J. Biol. Inorg. Chem.* **2012**, *17*, 927−938.
(88) Xu, L.; Gao, K.; Bao, C.; Wang, X. Combining Conformational Sampling and Selection to Identify the Binding Mode of Zinc-Bound Amyloid Peptides with Bifunctional Molecules. *J. Comput. Aid. Mol. Des.* **2012**, *26*, 963−976.
(89) Pan, L.; Patterson, J. C. Molecular Dynamics Study of Zn(Aβ) and $Zn(A\beta)_2$. *PLoS One* **2013**, *8*, e70681.
(90) Miller, Y.; Ma, B.; Nussinov, R. Zinc Ions Promote Alzheimer Aβ Aggregation via Population Shift of Polymorphic States. *Proc. Natl. Acad. Sci. U. S. A.* **2010**, *107*, 9490−9495.
(91) Xu, L.; Chen, Y.; Wang, X. Assembly of Amyloid β Peptides in the Presence of Fibril Seeds: One-Pot Coarse-Grained Molecular Dynamics Simulations. *J. Phys. Chem. B* **2014**, *118*, 9238−9246.
(92) Sugita, Y.; Okamoto, Y. Replica-Exchange Molecular Dynamics Method for Protein Folding. *Chem. Phys. Lett.* **1999**, *314*, 141−151.
(93) Mitsutake, A.; Sugita, Y.; Okamoto, Y. Generalized-Ensemble Algorithms for Molecular Simulations of Biopolymers. *Biopolymers* **2001**, *60*, 96−123.
(94) Xu, L.; Chen, Y.; Wang, X. Dual Effects of Familial Alzheimer's Disease Mutations (D7H, D7N, and H6R) on Amyloid β Peptide: Correlation Dynamics and Zinc Binding. *Proteins* **2014**, *82*, 3286−3297.
(95) Faller, P. Copper and Zinc Binding to Amyloid-β: Coordination, Dynamics, Aggregation, Reactivity and Metal-Ion Transfer. *ChemBioChem.* **2009**, *10*, 2837−2845.
(96) Hornak, V.; Abel, R.; Okur, A.; Strockbine, B.; Roitberg, A.; Simmerling, C. Comparison of Multiple Amber Force Fields and Development of Improved Protein Backbone Parameters. *Proteins* **2006**, *65*, 712−725.
(97) Jorgensen, W. L.; Madura, J. D. Quantum and Statistical Mechanical Studies of Liquids. 25. Solvation and Conformation of Methanol in Water. *J. Am. Chem. Soc.* **1983**, *105*, 1407−1413.
(98) Lührs, T.; Ritter, C.; Adrian, M.; Riek-Loher, D.; Bohrmann, B.; Dobeli, H.; Schubert, D.; Riek, R. 3D structure of Alzheimer's Amyloid-β(1−42) Fibrils. *Proc. Natl. Acad. Sci. U. S. A.* **2005**, *102*, 17342−17347.
(99) Pierce, B. G.; Wiehe, K.; Hwang, H.; Kim, B. H.; Vreven, T.; Weng, Z. ZDOCK Server: Interactive Docking Prediction of Protein-Protein Complexes and Symmetric Multimers. *Bioinformatics* **2014**, *30*, 1771−1773.
(100) Case, D. A.; Darden, T. A.; Cheatham, T. E.; Simmerling, C. L.; Wang, J.; Duke, R. E.; Luo, R.; Walker, R. C.; Zhang, W.; Merz, K. M.; Roberts, B.; Hayik, S.; Roitberg, A.; Seabra, G.; Swails, J.; Goetz, A. W.; Kolossváry, I.; Wong, K. F.; Paesani, F.; Vanicek, J.; Wolf, R. M.; Liu, J.; Wu, X.; Brozell, S. R.; Steinbrecher, T.; Gohlke, H.; Cai, Q.; Ye, X.; Wang, J.; Hsieh, M.-J.; Cui, G.; Roe, D. R.; Mathews, D. H.; Seetin, M. G.; Salomon-Ferrer, R.; Sagui, C.; Babin, V.; Luchko, T.; Gusarov, S.; Kovalenko, A.; Kollman, P. A. *AMBER 12*; University of California, San Francisco, 2012.
(101) Kollman, P. A.; Massova, I.; Reyes, C.; Kuhn, B.; Huo, S. H.; Chong, L.; Lee, M.; Lee, T.; Duan, Y.; Wang, W.; Donini, O.; Cieplak, P.; Srinivasan, J.; Case, D. A.; Cheatham, T. E. Calculating Structures and Free Energies of Complex Molecules: Combining Molecular Mechanics and Continuum Models. *Acc. Chem. Res.* **2000**, *33*, 889−897.
(102) Hou, T.; Wang, J.; Li, Y.; Wang, W. Assessing the Performance of the MM/PBSA and MM/GBSA Methods. 1. The Accuracy of Binding Free Energy Calculations Based on Molecular Dynamics Simulations. *J. Chem. Inf. Model.* **2011**, *51*, 69−82.
(103) Ball, K. A.; Phillips, A. H.; Wemmer, D. E.; Head-Gordon, T. Differences in β-Strand Populations of Monomeric Aβ40 and Aβ42. *Biophys. J.* **2013**, *104*, 2714−2724.
(104) Pettersen, E. F.; Goddard, T. D.; Huang, C. C.; Couch, G. S.; Greenblatt, D. M.; Meng, E. C.; Ferrin, T. E. UCSF Chimera-A Visualization System for Exploratory Research and Analysis. *J. Comput. Chem.* **2004**, *25*, 1605−1612.
(105) Iannuzzi, C.; Adrover, M.; Puglisi, R.; Yan, R.; Temussi, P. A.; Pastore, A. The Role of Zinc in the Stability of the Marginally Stable Iscu Scaffold Protein. *Protein Sci.* **2014**, *23*, 1208−1219.
(106) Qi, R.; Luo, Y.; Ma, B.; Nussinov, R.; Wei, G. Conformational Distribution and α-Helix to β-Sheet Transition of Human Amylin Fragment Dimer. *Biomacromolecules* **2014**, *15*, 122−131.
(107) Barz, B.; Olubiyi, O. O.; Strodel, B. Early Amyloid β-Protein Aggregation Precedes Conformational Change. *Chem. Commun.* **2014**, *50*, 5373.
(108) Pannuzzo, M.; Raudino, A.; Milardi, D.; La Rosa, C.; Karttunen, M. α-Helical Structures Drive Early Stages of Self-Assembly of Amyloidogenic Amyloid Polypeptide Aggregate Formation in Membranes. *Sci. Rep.* **2013**, *3*, 2781.
(109) Chen, Y. R.; Huang, H. B.; Chyan, C. L.; Shiao, M. S.; Lin, T. H.; Chen, Y. C. The effect of Aβ Conformation on the Metal Affinity and Aggregation Mechanism Studied by Circular Dichroism Spectroscopy. *J. Biochem.* **2006**, *139*, 733−740.
(110) Ma, B.; Nussinov, R. Polymorphic C-terminal β-Sheet Interactions Determine the Formation of Fibril or Amyloid β-Derived Diffusible Ligand-Like Globulomer for the Alzheimer Aβ42 Dodecamer. *J. Biol. Chem.* **2010**, *285*, 37102−37110.
(111) Yu, X.; Zheng, J. Polymorphic Structures of Alzheimer's β-Amyloid Globulomers. *PLoS One* **2011**, *6*, e20575.
(112) Rajadas, J.; Liu, C. W.; Novick, P.; Kelley, N. W.; Inayathullah, M.; LeMieux, M. C.; Pande, V. S. Rationally Designed Turn Promoting Mutation in the Amyloid-β Peptide Sequence Stabilizes Oligomers in Solution. *PLoS One* **2011**, *6*, e21776.
(113) Doran, T. M.; Anderson, E. A.; Latchney, S. E.; Opanashuk, L. A.; Nilsson, B. L. Turn Nucleation Perturbs Amyloid β Self-Assembly and Cytotoxicity. *J. Mol. Biol.* **2012**, *421*, 315−328.
(114) Roychaudhuri, R.; Lomakin, A.; Bernstein, S.; Zheng, X. Y.; Condron, M. M.; Benedek, G. B.; Bowers, M.; Teplow, D. B. Gly25-Ser26 Amyloid β-Protein Structural Isomorphs Produce Distinct Aβ42 Conformational Dynamics and Assembly Characteristics. *J. Mol. Biol.* **2014**, *426*, 2422−2441.
(115) Sarkar, B.; Mithu, V. S.; Chandra, B.; Mandal, A.; Chandrakesan, M.; Bhowmik, D.; Madhu, P. K.; Maiti, S. Significant Structural Differences between Transient Amyloid-β Oligomers and Less-Toxic Fibrils in Regions Known to Harbor Familial Alzheimer's Mutations. *Angew. Chem., Int. Ed.* **2014**, *53*, 6888−6892.
(116) Mithu, V. S.; Sarkar, B.; Bhowmik, D.; Chandrakesan, D.; Maiti, S.; Madhu, P. K. Zn++ Binding Disrupts the Asp23-Lys28 Salt Bridge without Altering the Hairpin Shaped Cross-β Structure of Aβ42 Amyloid Aggregates. *Biophys. J.* **2013**, *105*, 829−829.
(117) Mirecka, E. A.; Shaykhalishahi, H.; Gauhar, A.; Akgul, S.; Lecher, J.; Willbold, D.; Stoldt, M.; Hoyer, W. Sequestration of a β-Hairpin for Control of α-Synuclein Aggregation. *Angew. Chem., Int. Ed.* **2014**, *53*, 4227−4230.
(118) Hopping, G.; Kellock, J.; Caughey, B.; Daggett, V. Designed Trpzip-3 β-Hairpin Inhibits Amyloid Formation in Two Different Amyloid Systems. *ACS Med. Chem. Lett.* **2013**, *4*, 824−828.

DOI: 10.1021/acs.jcim.5b00063
J. Chem. Inf. Model. 2015, 55, 1218−1230